Plastic Pyrolysis over HZSM-5 Zeolite and Fluid Catalytic Cracking Catalyst under Ultra-Fast Heating

Wong, S. L., Armenise, S., Nyakuma, B. B., Bogush, A., Towers, S., Lee, C. H., Wong, K. Y., Lee, T. H., Rebrov, E. & Muñoz, M.

DOI 10.1016/j.jaap.2022.105793
ISSN 0165-2370
ESSN 1873-250X

Publisher: Elsevier

Journal of Analytical and Applied Pyrolysis 169 (2023) 105793

Contents lists available at ScienceDirect

Journal of Analytical and Applied Pyrolysis

journal homepage: www.elsevier.com/locate/jaap

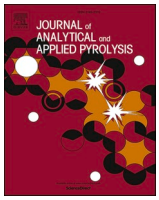

Plastic pyrolysis over HZSM-5 zeolite and fluid catalytic cracking catalyst under ultra-fast heating

Syie Luing Wong [a,b], Sabino Armenise [a], Bemgba Bevan Nyakuma [c], Anna Bogush [d], Sam Towers [d], Chia Hau Lee [e], Keng Yinn Wong [f], Ting Hun Lee [e,g], Evgeny Rebrov [b,h], Marta Muñoz [a,*]

[a] Dpto. Matemática Aplicada, Ciencia e Ingeniería de Materiales y Tecnología Electrónica, Universidad Rey Juan Carlos, C/ Tulipán s/n, Móstoles, 28933 Madrid, Spain
[b] School of Engineering, University of Warwick, Coventry CV4 7AL, United Kingdom
[c] UTM Centre for Low Carbon Transport (LoCARtic), Universiti Teknologi Malaysia, 81310 Skudai, Johor, Malaysia
[d] Centre for Agroecology, Water and Resilience (CAWR), Coventry University, Coventry CV4 7AL, United Kingdom
[e] Faculty of Chemical and Energy Engineering, Universiti Teknologi Malaysia, 81310 Skudai, Johor, Malaysia
[f] Faculty of Mechanical Engineering, Universiti Teknologi Malaysia, 81310 Skudai, Johor, Malaysia
[g] Innovation Centre in Agritechnology (ICA), Universiti Teknologi Malaysia, 84600 Muar, Johor, Malaysia
[h] Department of Chemical Engineering and Chemistry, Eindhoven University of Technology, P.O. Box 513, 5600 MB Eindhoven, the Netherlands

ARTICLE INFO

Keywords:
Tertiary recycling
Alternating magnetic field
Process intensification
Brønsted acidity
HZSM-5
Circular economy

ABSTRACT

Plastic pollution compromises the environment and human well-being, and a global transition to a circular economy of plastics is vital to address this challenge. Pyrolysis is a key technology for the end-of-life recycling of plastics, although high energy consumption limits the economic feasibility of the process. Various research has shown that the application of induction heating in biomass pyrolysis reduces energy consumption when compared to conventional heating. Nevertheless, the potential of induction heating in plastic pyrolysis is rarely explored. This paper presents an exploratory study on the thermal and catalytic pyrolysis of high-density polyethylene, low-density polyethylene, and polypropylene in a fixed bed reactor through induction heating. An MFI-type HZSM-5 zeolite (SiO_2/Al_2O_3 = 23) and an FAU-type spent fluid catalytic cracking (FCC) catalyst with distinctive Brønsted acidity and textural properties were used. A complete conversion of the plastic feedstocks was achieved within 10 min, even without a catalyst. Thermal pyrolysis produced wax (72.4–73.9 wt%) and gas products, indicating a limited degree of polymer cracking. Catalytic pyrolysis over HZSM-5 and FCC catalyst significantly improved polymer cracking, leading to higher gas (up to 75.2 wt%) and liquid product (up to 35.9 wt%) yields at the expense of wax yield (up to 25.4 wt%). In general, the gas products were rich in C3 and C4 compounds. The liquid product composition was highly dependent on the catalyst properties, for example, the HZSM-5 produced high aromatics, while the FCC catalyst produced high alkenes in the liquid products. The catalyst acidity and textural properties played an essential role in plastic pyrolysis within the short reaction time. This study demonstrated the feasibility of a fast, energy-efficient, and versatile plastic valorization technology based on the application of induction heating, where the plastic feed can be converted into wax, gas, and liquid products depending on the end-use applications.

1. Introduction

The excessive consumption of single-use plastics in the age of consumerism has generated a staggering amount of global plastic production. The short service life of these highly durable plastics creates enormous pressure on municipal waste management systems. Experts estimate an increase in global plastic waste production from 240 Mt/y in 2016–430 Mt/y in 2040 in a business-as-usual scenario [1]. This data translates to the outflow of ~1.71 and ~0.75 billion metric tonnes of plastic waste into the aquatic and terrestrial environment by 2020–2040 [1]. Sufficient evidence has demonstrated the possible trophic transfer of the fragmented plastic waste through the aquatic food web, causing an increased risk of toxicity to humans as one of the top predators [2]. Scientists have also pointed out that plastics may hinder the carbon

* Corresponding author.
E-mail address: marta.munoz@urjc.es (M. Muñoz).

https://doi.org/10.1016/j.jaap.2022.105793
Received 25 July 2022; Received in revised form 14 October 2022; Accepted 13 November 2022
Available online 17 November 2022

sequestration ability of phytoplankton and zooplankton, hence impeding the role of oceans as the most significant carbon sink on Earth [3]. Therefore, immediate actions are needed to handle the increasing amount of plastic waste, especially the unrecyclable ones. While the gradual bans of single-use plastics could serve as a temporary solution to the crisis, a paradigm shift from a linear to a circular economy of plastics is regarded as a sustainable solution in the long term without compromising the societal benefits of plastics [4,5].

At present, there are nearly 28 technology providers around the world that have developed or are currently developing thermal-chemical recycling technologies to promote the circular economy of plastics [6]. Pyrolysis is one of the key technologies used by these providers, where the plastic waste is degraded in an inert environment at high temperatures (400–600 °C) to produce value-added products, including liquid fuels, chemical feedstock, and carbon nanomaterials [7,8]. Given its strategic importance, plastic waste pyrolysis is an essential component in the SuSChem Strategic Innovation and Research Agenda which requires alignment of all actors in the innovation ecosystems [9]. At present, the technological readiness level of plastic pyrolysis stands at 6–7 [10]. Despite the significant progress in plastic pyrolysis development, several important issues limit the potential of large-scale plastic waste pyrolysis. As plastic pyrolysis is an endothermic reaction, the significant energy cost in the scaled-up process reduces the cost-competitiveness of the pyrolysis oil against the fossil-based oil. Most research teams utilized resistive heating in plastic pyrolysis, which is associated with low heating and cooling rates, and therefore low energy efficiency. This limitation is responsible for the high energy consumption and thus aforementioned low economic viability of large-scale plastic waste recycling. A potential solution to this challenge lies in replacing resistive heating with induction heating, which is a non-contact technique involving the induction of eddy current on the surface of a ferromagnetic metal placed in an alternating magnetic field. The eddy current generates the Joule heating effect, which leads to rapid heat generation of the metal. As most plastic pyrolysis reactors are made of stainless steel (which is a good susceptor in an alternating magnetic field), the application of induction heating in plastic pyrolysis could be a critical and innovative solution to achieve higher energy efficiency and, therefore, higher economic feasibility for large-scale application.

Several research teams have investigated induction heating in biomass waste pyrolysis. Tsai et al. [11] reported the pyrolysis of biomass wastes to bio-oils in a stainless-steel reactor via induction heating. Muley et al. [12] also developed a two-stage reactor for the pyrolysis of pinewood sawdust with induction heating applied to biomass pyrolysis and catalytic upgrading stages. Compared to resistive heating, the adoption of induction heating in the catalysis stage lowered the degree of coke deposition in catalyst particles. This observation was related to a more efficient heat transfer from the stainless-steel reactor surface (susceptor) to the catalyst bed during the induction heating process. The pyrolysis of electronic waste through induction heating (with graphite crucible as susceptor) also led to a more significant weight reduction (by 7 %) than pyrolysis through resistive heating [13]. Compared with biomass pyrolysis, scientific investigations on the roles of induction heating in plastic pyrolysis are limited in the literature. Nakanoh et al. [14] were the first team who mentioned the feasibility of the process. However, no information was provided on the plastic pyrolysis product yields and compositions. Zeaiter [15] reported on the rapid decomposition of high-density polyethylene waste via induction heating during pyrolysis, resulting in insufficient contact between the pyrolysis intermediates and catalyst particles. This phenomenon ultimately led to high wax/liquid and solid yields but low gas yields. To date, there is an insufficient understanding of the feasibility of plastic pyrolysis via induction heating. To fill this knowledge gap, an exploratory study was performed to investigate the thermal and catalytic pyrolysis of neat plastics in a self-fabricated stainless-steel (SS316) fixed bed reactor using induction heating. Specifically, the effects of catalyst properties on the product yields and compositions from the pyrolysis of low-density polyethylene (LDPE), high-density polyethylene (HDPE), and polypropylene (PP) pellets in a nitrogen environment were investigated. This is the first study that reports the behaviors of thermal and catalytic pyrolysis of different polymers via induction heating of the reactor wall, which will provide valuable insights into novel strategies for plastic waste valorization.

2. Methodology

2.1. Materials

The LDPE, HDPE, and PP pellets (particle size: 3–5 mm) were supplied by a Spanish energy and petrochemical company and were used as received. For catalytic pyrolysis, ZSM-5 catalyst (CBV 2314, Zeolyst International, $SiO_2/Al_2O_3 = 23$) and spent fluid catalytic cracking (FCC) catalyst obtained from a Spanish-based international energy company were used. Before the experiments, the catalysts were calcined at 550 °C in the air for 3 h to remove all the adhered impurities (including moisture) [16]. The calcination step also converts the ZSM-5 zeolite from ammonium form to hydrogen form [17] and removed the coke formed on the FCC catalyst.

2.2. Materials characterizations

The thermal degradation behavior of the plastics was analysed using a thermogravimetric analyser (TGA, STAR system, Mettler Toledo). The samples were purged with pure nitrogen gas (20 mL/min) and then heated at 10 °C/min in the temperature range of 25–800 °C [18]. The raw TGA data were differentiated to obtain the derivative (DTG) curves for the samples. The molecular weight distribution (MWD), molecular weight averages (M_w), and polydispersity indexes (PI) of the plastic pellets and waxes from thermal pyrolysis were determined using gel-permeation chromatography (GPC) coupled with infrared detector (GPC-IR6) (Polymer Char, Spain) [19]. The samples were prepared by dissolving approximately 10 mg of plastics in 1 mL of 1,2-dichlorobenzene at 150 °C, followed by in-line filtration. The M_w and PI values referred to the monodisperse PS standards [19].

The density and strength of the Brønsted acidic sites on the catalysts were characterized based on the thermogravimetric measurement of temperature-programmed decomposition of *n*-propylamine (NPA) in a DSC-TGA thermal analyser (Model: SDT Q600, TA Instruments) [20]. The sample was heated at 600 °C for 30 min in nitrogen flow (30 mL/min) to remove all absorbed impurities and then saturated with NPA at 150 °C. After that, the sample was heated in nitrogen flow (30 mL/min) at 150–700 °C with a heating rate of 10 °C/min. The textural properties of the catalysts were characterized based on the nitrogen adsorption-desorption isotherm produced by the Micromeritics Gemini 2360 instrument at −196 °C [21]. Before the analysis, the samples were outgassed at 350 °C for 4 h. The surface area of the samples was computed using the Brunauer-Emmett-Teller's (BET) equation from the nitrogen adsorption curve in the region $0.05 \leq P/P_o \leq 0.3$. The pore size distributions of HZSM-5 and FCC catalysts were computed using the Barrett-Joyner-Halenda (BJH) method from the desorption isotherms. The XRD diffractograms were recorded on a Panalytical X'Pert Pro (The Netherlands) using Cu Kα radiation generated at 45 kV and 40 mA. A scanning range from 5° to 100° was used at a speed of 0.03°/s.

2.3. Reactor system for plastic pyrolysis

A fixed bed reactor system (Fig. 1) was used for plastic pyrolysis through induction heating. The reactor was an AISI 316 stainless steel tube (length, L: 10.0 cm, outer diameter, OD: 2.2 cm). The plastic pellets and the catalysts were placed in the middle section of the reactor between the layers of quartz wool. The reactor also acted as a susceptor in an alternating magnetic field produced by a 3-turn copper coil (L: 5.0 cm, inner diameter, ID.: 4.5 cm) connected to an induction heater

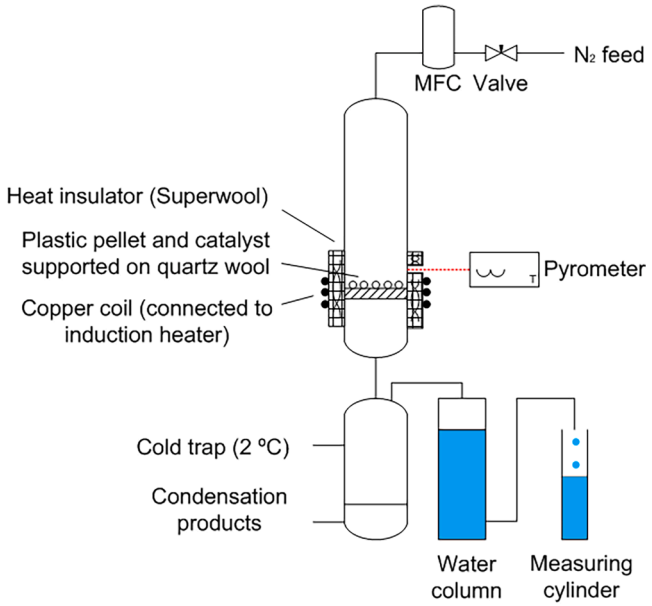

Fig. 1. Schematic diagram of the plastic pyrolysis system (not drawn to scale).

(Easyheat system, Ambrell, UK) with an output power of 1.2 kW. The current frequency was fixed at 315 kHz. A Superwool Plus fiber (13 mm) layer was placed in between the reactor and copper coil to reduce heat losses from the reactor wall to the surrounding. The reactor wall temperature was measured using a pyrometer (CTM-3CF75H1-C3, Micro-Epsilon) via a small opening in the insulation layer.

The top part of the reactor was welded to an inlet AISI 316 tube (L: 5.0 cm, OD: 2.5 cm), while the bottom part was welded to an outlet AISI 316 tube (L: 5.0 cm, OD: 1.8 cm). A stainless-steel cold trap connected to the bottom reactor outlet was maintained at 2 °C to collect the condensable reaction products. The non-condensable gases were collected in a water column placed after the cold trap. The total volume of the gas product evolved during plastic pyrolysis was determined based on the volume of water displaced from the water column into a measuring cylinder.

2.4. Plastic pyrolysis process

In this exploratory study, 1.00 g of plastic pellets (LDPE, HDPE, or PP), together with 0.20 g of catalyst (in the case of catalytic pyrolysis), were placed on 0.20 g of a quartz wool layer in the reactor. As a basis to estimate the effect of the catalyst, a series of blank experiments were carried out, hereafter termed "thermal pyrolysis" in this paper. Before the pyrolysis process, the reactor system was purged with nitrogen gas (120 mL/min) for 10 min to prevent the oxidation/combustion of the plastics during pyrolysis. Next, the nitrogen gas flow was turned off. The induction heater was turned on for 30 min to allow reactor heating. After 30 min, the induction heater was turned off, and the reactor was allowed to cool to room temperature. If the wax product was formed in the cold trap, the wax was collected and weighed. If a liquid product was formed, it was extracted with 3 mL of dichloromethane before being weighed and analysed. All the pyrolysis experiments were performed in duplicates. The average values and per cent errors of product yields are presented in Section 3. In general, the experimental errors fall within 7%.

According to the temperature measurement results (Section S1, Supplementary materials), induction heating successfully raised the reactor temperatures to 500–700 ℃ within 10 min. The heating rate of the system is estimated to be 50–85 ℃/min depending on the induction heater power. By definition, the system/process could be classified as fast pyrolysis, which has a typical heating rate of 10–200 ℃/min [22]. Based on the temperature measurement results, the plastic pyrolysis experiments occurred at 650 °C to allow full plastic conversion.

2.4.1. Determination of product yield

As discussed in Section 2.4 and Section S1 (Supplementary materials), the heating power of the induction heater was selected to ensure the complete conversion of the plastic pellets in all experiments. Consequently, no plastic remained in the reactor after pyrolysis reactions. The liquid yield was calculated based on the following equation:

$$Liquid\ yield, x_l \quad (\%) = \frac{m_l}{m_p} \times 100\% \tag{1}$$

where mL (g) is the liquid product mass, and mp (g) is the mass of the plastic pellet used. Similarly, the wax yield was calculated based on the mass of the wax product collected. The amount of coke formed on the catalyst was characterized using the temperature-programmed oxidation (TPO) technique described in the literature [23]. The spent catalyst (10 mg) was heated to 800 °C using a thermo-gravimetric analyser (TGA/DSC STAR system, Mettler) at a heating rate of 15 °C/min, followed by a hold for 10 min at 800 °C, with an airflow rate of 100 mL/min. The analysis result was used to calculate the total mass of coke formed on the catalyst. The coke yield was then calculated using the following equation:

$$Coke\ yield, x_c(\%) = \frac{m_c}{m_p} \times 100\% \tag{2}$$

where mc (g) is the total mass of coke formed.

2.5. Products characterization

The light hydrocarbon compounds in the gas products were analysed using the Shimadzu 2010 GC equipped with an FID column (Equity-1 column, Supelco, L: 50 m, ID: 0.53 mm, stationary phase: poly(dimethylsiloxane), film thickness: 3 μm). Helium gas (31 mL/min) was used as carrier gas. The heating program used was: 50 °C for 6 min, then increased to 238 °C at 12.5 °C/min, and then held for 5 min. The split ratio was 2.0. Both the injector temperature and detector temperature were maintained at 250 °C. The abundance of hydrocarbon compounds in the gas products was reported according to the carbon numbers [24,25]. The chemical composition of the liquid products was analysed using the Thermo Scientific™ Q Exactive™ GC Orbitrap™ GC-MS/MS System with a method adapted from the literature [26]. The GC-MS/MS system was equipped with the Thermo Scientific TG-5SILMS capillary column (internal diameter: 0.25 mm, length: 30 m, film thickness: 0.25 μm, PN 26096–1420). Helium (1.2 mL/min) was used as a carrier gas. The injector was operated at 280 °C, with a split ratio of 25:1. The oven was initially maintained at 40 °C for 2 min, then heated up to 320 °C at a ramp rate of 30 °C/min, and finally held at 320 °C for 15 min. The MS was equipped with an electron ionization source (ionization voltage = 70 eV, m/z = 50–600). The ion source and transfer line were operated at 280 °C and 150 °C, respectively. The peaks in the total ion chromatogram were identified using Xcalibur Qual Browser software (Xcalibur version 4.2.47) by mass spectra searching the National Institute of Standards and Technology (NIST) Mass Spectral Search Program for the NIST/EPA/NIH EI and NIST Tandem Mass Spectral Library Version 2.3. The C7-C40 alkanes standard (1000 μg/mL) purchased from Sigma Aldrich was used to facilitate hydrocarbon compound identification in the liquid products.

3. Results and discussion

3.1. Plastics characterization

Information on the thermal behavior of the plastics is essential to determine suitable pyrolysis process conditions. Fig. 2a shows the TGA

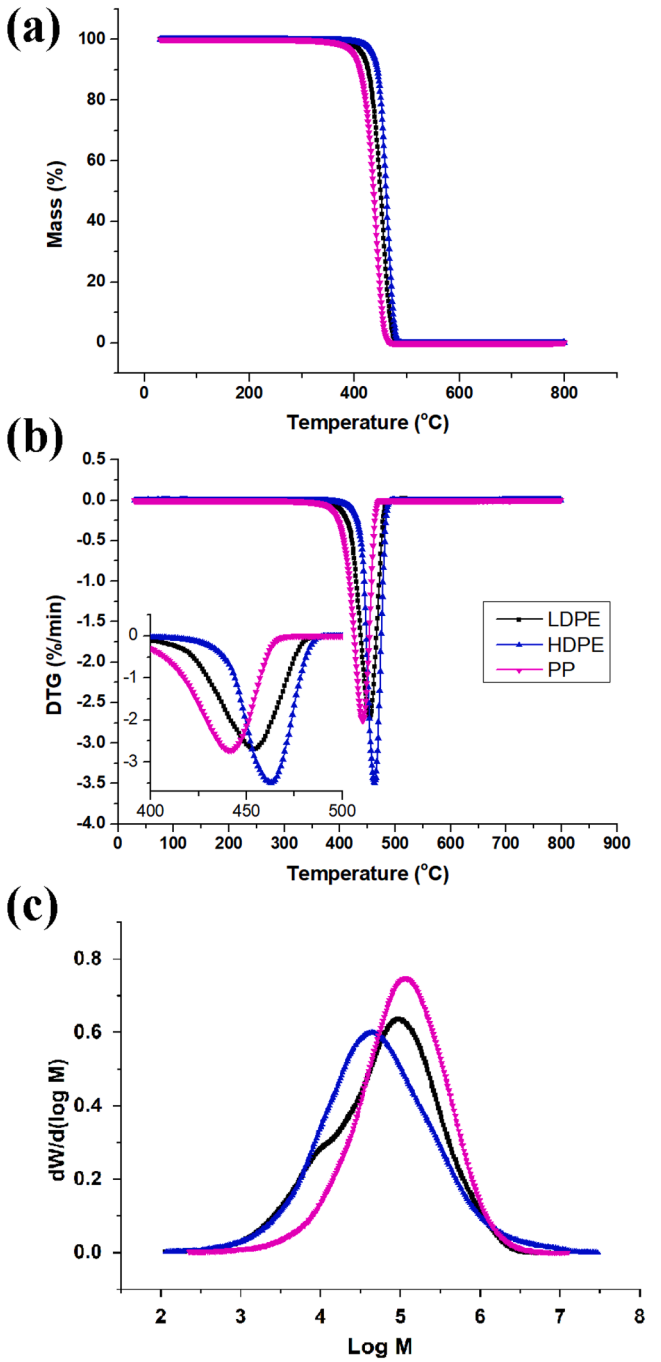

Fig. 2. (a) TG and (b) DTG plots, together with (c) MWD of the plastic samples used in this study.

curves of LDPE, HDPE, and PP. In general, all the samples exhibited a one-step mass-loss process, which is a typical degradation behavior observed in other clean plastic samples [27]. The samples contain negligible moisture evidenced by the absence of a peak at ~100 °C in the TGA plots. Complete degradation of all plastics occurred within the range of 435–500 °C. The decomposition peak temperatures of the plastics are observed in the following order: PP (458 °C) < LDPE (471 °C) < HDPE (482 °C) (Fig. 2b). Although PP, LDPE and HDPE consist of long hydrocarbon chains, the presence of methyl groups in the PP polymer chain lowers its thermal stability when compared to PE samples [28]. The lower decomposition temperature of LDPE compared to HDPE is related to the higher degree of branching in the former polymer [29].

GPC is another critical analysis that provides information on the MWD of the polymer samples. The MWD of the plastic samples is shown in Fig. 2c, while the numerical values of mass average (M_w), number average (M_n), and Z average (M_z) molecular masses of the samples are provided in Table 1. All the samples display single modal peaks, which is similar to the observations made by Cáceres et al. [30] and Zhang et al. [31]. LDPE and HDPE exhibit broader peaks, indicating wider MWD [32]. This observation is accompanied by high PI values (13.4 and 16.8 respectively, Table 1). In comparison, PP produced smaller and higher peaks, with PI values of 6.62. The M_n of the samples is arranged in the following order: LDPE (12600) <HDPE (13300) < PP (32443). These values are very different from those measured in other works [33], as neat plastics properties are often adjusted by the manufacturers for different industrial applications.

3.2. Catalyst characterization

The Brønsted acidic sites in zeolitic catalysts play an important role as proton donors during the catalytic cracking of hydrocarbons [34], including plastic decomposition products [35], into smaller hydrocarbons. The Brønsted acidic sites in zeolites originate from the protons that balance the negative charges due to the substitution of Si by Al atoms in the zeolitic framework. The abundance of Brønsted acidic sites typically increases with aluminum content, which is represented by the Si/Al ratio of the zeolitic catalysts. When a catalyst saturated with NPA is heated, the Brønsted acidic sites catalyze NPA decomposition into propene and ammonia at a stoichiometric ratio via the Hoffmann elimination reaction [36], enabling estimation of the Brønsted acidic sites density on the catalyst. The strengths of the acidic sites can be estimated based on the product evolution peak temperature(s) [36]. Xian et al. [34] demonstrated different accessibility of the Brønsted acidic sites in a zeolite sample, related to their locations in the crystal grains.

As shown in Fig. 3a, HZSM-5 exhibits three peaks at different temperatures. The peaks observed at 400 °C and 460 °C are attributed to the evolution of products from NPA decomposition on Brønsted acidic sites. The peak temperatures observed in this study closely match the HZSM-5 samples used by Xian et al. [34] and Xian et al. [36] (410–420 °C and 470–490 °C respectively), as well as the HZSM-5 sample prepared by Caeiro et al. [37] (415 °C and 485 °C respectively). The peak at 400 °C denotes the presence of stronger Brønsted acidic sites that can catalyze NPA decomposition at a lower temperature. In contrast, the peak at 460 °C represents weaker Brønsted acidic sites that can catalyze NPA decomposition at higher temperatures. A broad peak at 280 °C exists due to the desorption of physisorbed NPA from weak acidic sites, which was also observed by Xian et al. [36]. Previous works by other teams indicate that desorption peaks below 300 °C represent acidic sites that are too weak to decompose NPA, and therefore unlikely to catalyze hydrocarbon cracking [38]. The integration of peak areas (excluding the peak at 280 °C) revealed a Brønsted acidic sites density of 1082.3 μmol/g_{cat} for HZSM-5 (in agreement with data reported by Losch et al. [39]), with 72.4 % contribution from the strong Brønsted acidic sites (Table 2). When compared to HZSM-5, the FCC catalyst exhibits only two peaks with very low intensity. Similar to HZSM-5, the peak displayed at 212 °C is attributed to the desorption of physisorbed NPA, while the peak at 416 °C is related to the desorption of NPA decomposition products. No additional peak is observed. The quantification of the area under peak (416 °C) indicates a Brønsted acidic sites density of

Table 1
Information of plastic characteristics extracted from GPC results.

Sample	LDPE	HDPE	PP
M_n (g/mol)	12,600	13,300	32,443
M_w (g/mol)	168,500	223,600	214,640
M_z (g/mol)	805,000	3,070,500	754,372
PI (M_W/M_n)	13.4	16.8	6.62

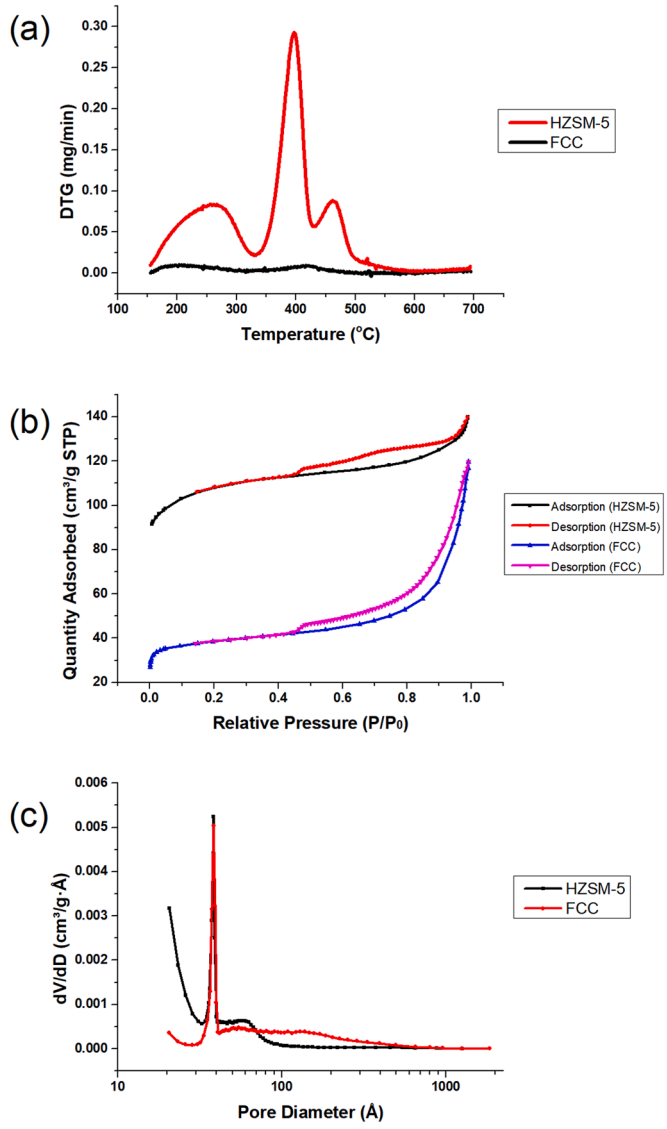

Fig. 3. (a) Brønsted acidity profile, (b) nitrogen adsorption-desorption isotherms and (c) pore size distribution curves of HZSM-5 and FCC catalyst.

Table 2
Textural characteristics and acidity properties of catalysts.

Property	HZSM-5	FCC catalyst
BET surface area (m^2/g)	410.6	147.5
Micropore volume (cm^3/g)	0.124	0.042
Micropore area (m^2/g)*	313.2	108.1
Mesopore area (m^2/g)	97.4	39.4
Total acidity ($\mu mol/g_{cat}$)	1082.3	100.5
Weak Brønsted acidic sites ($\mu mol/g_{cat}$)	298.8	100.5
Strong Brønsted acidic sites ($\mu mol/g_{cat}$)	783.4	0.0

* Calculated by the t-plot method

100.5 μmol/g_{cat}, contributed solely by weak Brønsted acidic sites. In addition to the Y zeolite, the fresh FCC catalyst also consists of binder and filler materials that improve the mechanical performance of the catalyst in the FCC process, while reducing the density of Brønsted acidic sites per unit catalyst mass. Furthermore, the spent FCC used in this study could be poisoned by transition metal contaminants, especially vanadium and nickel, during FCC operations [40,41], rendering a great number of active sites ineffective for cracking plastic pyrolysis intermediates in this study.

The textural property of a catalyst is another significant factor that influences product selectivity during the catalytic cracking of plastics [35]. The nitrogen adsorption-desorption isotherms and pore size distribution curves of HZSM-5 and FCC catalysts are shown in Fig. 3b,c. A combination of type II and type IV(a) isotherms is observed for both samples according to the updated classification standards of adsorption-desorption isotherms by IUPAC [42]. At low relative pressure ($0 \leq P/Po \leq 0.02$), the number of nitrogen molecules adsorbed increased quickly due to micropore filling and single-layer adsorption in the mesopores, leading to the convex shape of the curves. Further increase of relative pressure leads to multilayer adsorption. At $P/P_o \approx 0.44$, condensation of the adsorbate molecules occurs in the mesopores (capillary condensation). Due to the presence of macropores in the samples, adsorption saturation is not observed. The desorption curves of both samples do not coincide with their respective adsorption curves at $P/P_o \geq 0.44$, and different hysteresis loops are observed. The hysteresis loop for HZSM-5 is the H4 type, indicating a mixture of microporosity and mesoporosity dominated by narrow crack pores [43]. In contrast, an H3-type hysteresis loop is observed for the FCC catalyst indicating plate slit, crack, and wedge structures [44]. HZSM-5 possess a higher micropore area and mesopore areas (Table 2), thus a higher BET surface area (410.6 m^2/g) than those of FCC catalyst (147.5 m^2/g). Fig. 3c shows that HZSM-5 has a peak distribution below ~70 Å, with a single peak of 38 Å (3.8 nm), leading to a large micropore volume (0.124 cm^3/g) and small mesopore volume (0.082 cm^3/g). The observed pore distribution characteristic is typical for HZSM-5 zeolite [45]. FCC catalyst also produces a single peak with similar intensity to HZSM-5. Fig. 3b indicates a significant proportion of HZSM-5 zeolite in such a mixture. Nevertheless, the FCC catalyst has a wider pore distribution, up to 150 Å (15.0 nm), leading to a larger mesopore volume (0.131 cm^3/g). This is accompanied by a smaller micropore volume (0.042 cm^3/g). The average pore diameter based on the BJH desorption curve is 4.80 nm for HZSM-5, and 11.90 nm for the FCC catalyst.

The crystallinity and average crystallite size of the H-ZSM5 and the FCC catalyst is examined using the XRD technique. The H-ZSM5 sample (Fig. 4) depicts sharp peaks at $2\theta = 8.03°$, 8.97°, 13.24°, 13.99°, 16.06°, 23.11°, 24.01°, and 30.24°, which are related to (101), (111), (102), (112), (022), (051), (313) and (062) planes in the X-ray diffraction pattern of the MFI topology, indicated by the Powder Diffraction File (PDF) 01–079–1638 [46]. Similar diffraction patterns are also observed in the hierarchical ZSM-5 zeolite synthesized by Jesudoss et al. [47] and meta-promoted ZSM-5 zeolite characterized by [48]. When compared with HZSM-5 zeolite, FCC catalyst displays peaks with lower intensities. This is possibly attributed to the partial destruction of the FCC catalyst crystallinity after repeated usage in the FCC process. The diffraction lines exhibited by the FCC catalyst match the Y-type zeolite (PDF number: 01–077–1549), while the small peaks observed at 45.8° and 67.0° are attributed to the characteristic peaks of Al_2O_3 [49]. The average crystallite sizes of the HZSM-5 zeolite and the FCC catalyst were estimated to be 35.85 nm and 18.75 nm using the Debye Scherrer equation:

$$L = \frac{0.89 \quad \lambda}{\beta \cos\theta} \tag{3}$$

where L is the average crystallite size (nm), λ is the X-ray wavelength (0.154 Å), θ is the Bragg diffraction angle (in radian) and β is the full width at half maximum (FWHM) (in radian).

3.3. Thermal and catalytic pyrolysis of plastics

3.3.1. Product yields

The product yields for the thermal and catalytic pyrolysis of HDPE, LDPE, and PP are provided in Fig. 5. Thermal pyrolysis of plastics produced high wax yield (72.4–73.9 wt%). Two types of waxes were formed in each experimental run (regardless of the plastic type): white wax in

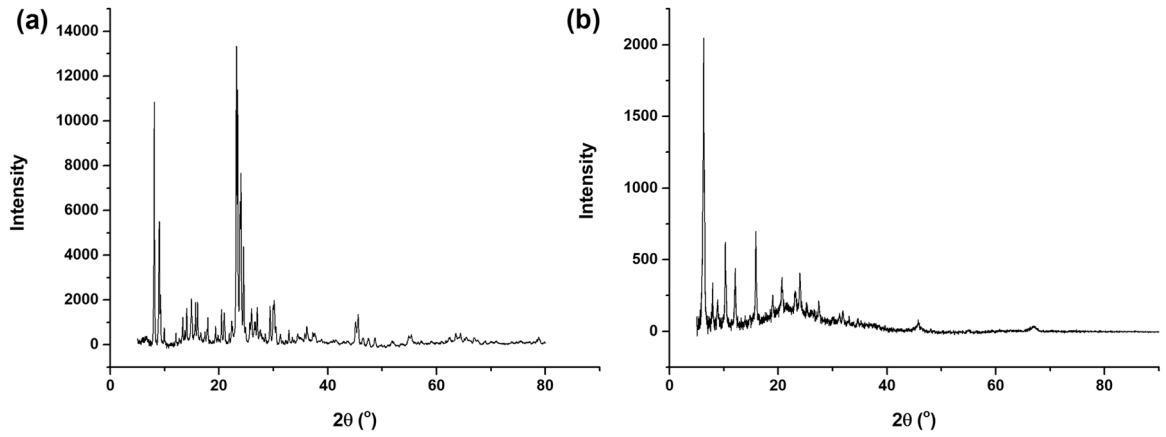

Fig. 4. X-ray diffractograms of (a) H-ZSM5 and (b) FCC catalyst.

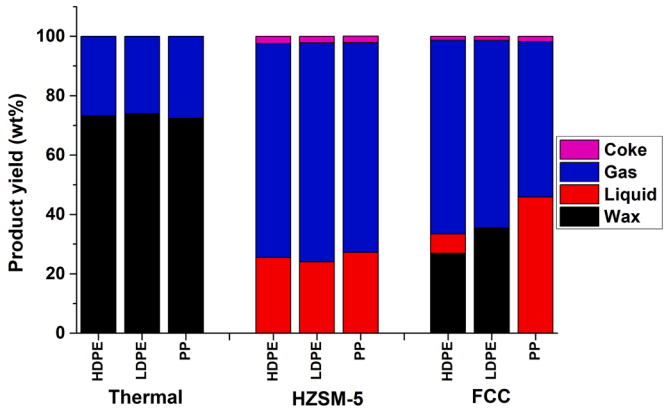

Fig. 5. Product yields from thermal and catalytic pyrolysis of plastics by induction heating.

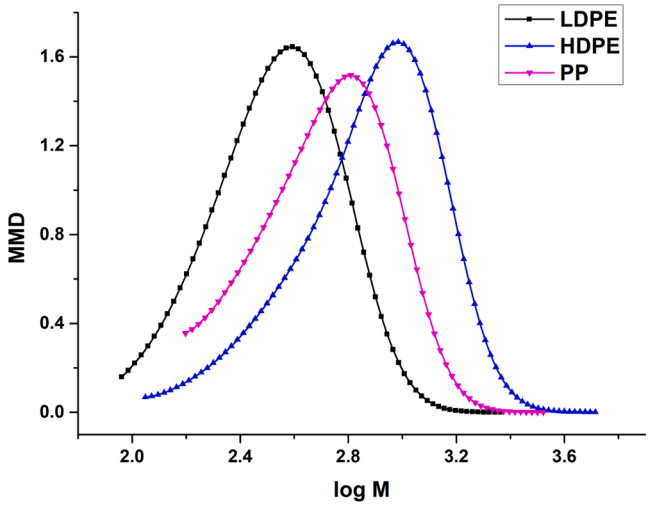

Fig. 6. Molecular weight distributions of waxes produced from thermal pyrolysis of LDPE, HDPE, and PP.

the cold trap and yellow/green wax in the tubing that connected the reactor to the cold trap (Fig. S2, Supplementary materials). This observation signifies the following: when thermal pyrolysis occurs, the plastic vapor fills up the reactor space rapidly. Most of the vapor exited the reactor (due to the volume expansion) and condensed in the cold trap as white wax. As no nitrogen gas flows through the reactor in the experiments, the residence time of the plastic vapor in the reactor was affected by the rate of plastic conversion. The plastic vapor that remained in the reactor was further cracked to form lighter molecules, which then condensed in the tubing as yellow/green wax. This observation is also supported by the production of non-condensable gases up to a reaction time of 30 min, even after the complete plastic conversion. The formation of wax products from plastics indicates the occurrence of random C-C bond scission along the polymer chain, resulting in fragments with high molecular weights. This is a typical observation for plastic pyrolysis in a continuous system with short residence time, for example, a fluidized bed reactor [50]. A longer residence time promotes extensive cracking of the intermediates, producing more gas products and fewer waxes [51]. All the wax samples displayed a single peak with narrower MWD (Fig. 6) compared to the plastic pellets samples in Fig. 2c. This is accompanied by low PI values (1.32–1.46). The M_w values of the wax samples are arranged in the following order: LDPE (400) < PP (600) < HDPE (900) (Table 3). Assuming these waxes consisted of -CH_2- groups [33], then these waxes contain chains with average carbon numbers of 28 (LDPE), 42 (PP) and 64 (HDPE). These data show that thermal pyrolysis within a short period is sufficient to reduce the molecular weight of the polymers to 1.5–4.5 % of their original molecular weights. When compared to the plastic pyrolysis waxes produced by

Table 3
Information on wax characteristics extracted from GPC results.

Sample	LDPE	HDPE	PP
M_n (g/mol)	300	600	500
M_w (g/mol)	400	900	600
M_z (g/mol)	500	1200	800
PI (M_W/M_n)	1.32	1.46	1.33

Arabiourrutia et al. [33], the waxes obtained in this study have smaller M_W and PI values. The observed difference could be ascribed to the higher heating rates used in this study.

The presence of catalysts in plastic pyrolysis reduced the wax yield while increasing the gas and liquid yields significantly. When HZSM-5 zeolite was used, all the plastics were converted to liquid products (24.0–27.2 wt%) and gas products (345.0–448.0 cm^3/g). A small number of cokes were also formed on the used zeolites, which is discussed further in Section 3.4. Despite the inferior textural properties (compared to HZSM-5) and absence of strong Brønsted acidic sites, the FCC catalyst demonstrated catalytic activity in plastic pyrolysis within a short reaction time. Nevertheless, the catalyst was unable to convert all the heavy hydrocarbons into smaller molecules, and the wax product was mixed with the liquid product in the cold trap. These observations show that catalysts can effectively reduce the activation energy of polymer cracking, which was also observed by Zhou et al. [51] in

microwave-assisted pyrolysis of plastic waste. Interestingly, plastic-type seems to influence the distribution of products during catalytic pyrolysis over FCC catalyst. LDPE produced soft wax and gas product without liquid products, while HDPE resulted in a mixture of soft wax and liquid products, together with the gas product. On the other hand, all the wax products from PP pyrolysis were converted into gas and liquid products. A different trend was observed in catalytic pyrolysis over HZSM-5, where the LDPE and HDPE showed closely similar product distribution compared to PP. Such differences could be related to the relatively weaker catalytic performance of the FCC catalyst (compared to HZSM-5), which influenced the product formation from HDPE and LDPE in different ways. More detailed investigations are necessary to fully understand the role of Brønsted acidic sites in the catalytic pyrolysis of plastics assisted by induction heating.

The application of induction heating in plastic pyrolysis using different reactor setups has been attempted by several research teams. Whajah et al. [52] reported LDPE pyrolysis over Fe_3O_4 mixed with Ni- or Pt-based catalysts (1:1 mass ratio for plastic to the Fe_3O_4/catalyst mixture) in a glass batch reactor. The Fe_3O_4 particles were heated to 350 ºC, and the pyrolysis reactions lasted for 120 min with 100 mL/min N_2 flow. Due to the small amount of heat generated by the metallic susceptor in the alternating magnetic field, a longer reaction time was needed to achieve 94 % plastic conversion, with gas yields of 15–80 wt %, liquid yields of 2–43 wt%, and coke yields of 1.3–2.4 wt%. In contrast, Hassani [53] performed LDPE pyrolysis over HZSM-5 zeolite via the induction heating of a semi-batch reactor wall to 400–500 ºC, with a catalyst loading of 9–25 wt%. The author reported gas yields of 60–75 wt%, liquid yields of 20–55 wt%, and coke yields of 2–4 wt%. Similar to the aforementioned works, this study demonstrated that catalytic pyrolysis of plastics produced high gas yields and comparatively low liquid yields. Nevertheless, induction heating of the reactor wall in this study generated a large amount of heat in a short time and ensured a total plastic conversion. The short pyrolysis time could also reduce the secondary reactions, leading to lower coke yields in this study compared to Whajah et al. [52] and Hassani [53].

3.3.2. *Evolution rates and composition of gas products*

To obtain further insights on the effects of induction heating on plastic pyrolysis behavior, the evolution rates of gas products during thermal and catalytic pyrolysis of HDPE, LDPE, and PP were recorded (Fig. 7). As plastic pyrolysis typically leads to the generation of light hydrocarbon gas, Fig. 7 indicates the plastic decomposition rate during pyrolysis powered by induction heating. In all experiments, rapid gas evolution was observed between 3 and 5 min (corresponding to the temperature of 450–550 °C). This observation is in line with the TGA data where plastic decomposition was observed at 450–510 °C (see Fig. 2a). In all experiments, the generation of gas products slowed down after the temperature reached 600 °C after 7 min. After 10 min, complete plastic conversion into volatile products occurred. The experiments were performed without inert gas flow to enable precise observation of the product gas evolution rates in different experimental runs. During the reactions, some of the gas products that remained in the reactor underwent further cracking to produce lighter hydrocarbons leading to a further increase in the product gas volume. The secondary cracking effects could be reduced when a sweeping gas is provided to remove the pyrolysis intermediates from the reactor during plastic pyrolysis.

In thermal pyrolysis (Fig. 7a), only a small amount of gas products (95–132 mL/g plastic) were produced, accompanied by wax formation, regardless of the plastic type (Fig. 6). Similar observations were made by Zeaiter [15], indicating the limited degree of polymer chain cracking during thermal pyrolysis. Several research teams reported that plastic pyrolysis with high heating rates (fast pyrolysis) produced more gas products, while pyrolysis with low heating rates (slow pyrolysis) produced more liquid products [54,55]. Fig. 7a also reveals higher product gas evolution (representing more extensive cracking) of PP compared to HDPE and LDPE, as PP (with a branched-chain structure and tertiary carbon) is more susceptible to C-C bond cleavage. Thus, PP can be cracked more easily than PE (linear structure with limited branching) to produce permanent gases, which is also supported by the TGA result (Fig. 2). Similar observations were also made for PP pyrolysis by resistive heating [56] and microwave heating [51].

The presence of catalysts significantly increased the product gas evolutions to different degrees (Fig. 7b, c). In the presence of HZSM-5, the gas production volumes increased more than trifolds (345–448 mL/g plastic) when compared to thermal pyrolysis. This is related to the high catalytic property of HZSM-5, which is extensively reported in plastic pyrolysis research. The microporous structure and high acidic properties of HZSM-5, as mentioned in Section 3.2, promoted a high degree of plastic cracking, leading to the formation of liquid products and more C1-C4 products. In comparison, catalytic pyrolysis over FCC catalyst produced a lower amount of gas products (164 −192 mL/g plastics). This is attributed to the less severe plastic cracking due to the lower acidity of the catalyst (Section 3.2).

Fig. 7b, c also reveals the lower degree of gas product evolution during catalytic cracking of PP compared to HDPE and LDPE, which is in contrast with the observation in Fig. 7a. Such observation is related to the limited contact between the PP molecules (with branched-chain structure) with the catalyst surface, leading to lower cracking and thus gas product volume. The steric hindrance effect in catalytic pyrolysis of PP was also observed by Li et al. [57] and Palza et al. [58].

Fig. 8 summarizes the composition of gas products from thermal and catalytic pyrolysis (in terms of carbon number), with the details of the gas components provided in Table S1 (Supplementary materials). The gas products from thermal pyrolysis are rich in C2 (12.63–18.27 %) and C3 (67.39–72.19 %) compounds. The presence of catalysts increased the abundance of C3 and C4 compounds to higher extents, at the expense of C1 and C2 compounds. The possible explanation for this observation is the reduced residence time of the plastic vapor in the reactor during catalytic pyrolysis. Due to the abundance of C3 compounds (propane and propene) and C4 compounds (butane and butene), the average molecular weight of the gas products was 41.87–46.67 (Table 4). The

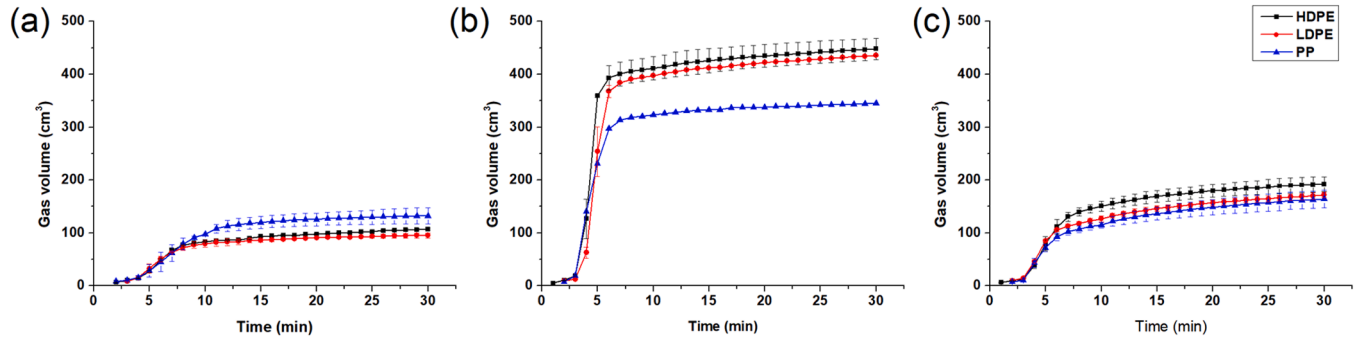

Fig. 7. Evolution rate of the gas product during (a) thermal pyrolysis and catalytic pyrolysis of plastics over (b) HZSM-5 and (c) FCC catalyst.

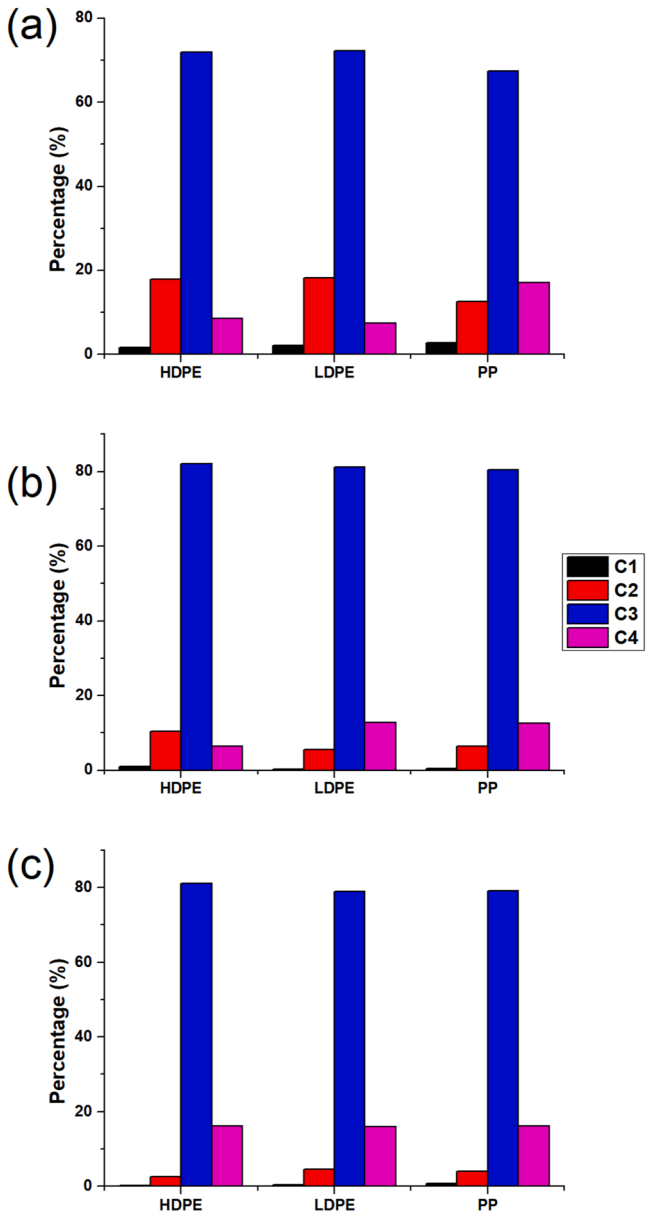

Fig. 8. Composition of gas products from (a) thermal pyrolysis and catalytic pyrolysis over (b) HZSM-5 and (c) FCC catalyst powered by induction heating.

Table 4
Average molecular weights of the gas products.

Plastic/catalyst	Average molecular weights (g/mol)
HDPE/thermal	42.23
LDPE/thermal	41.87
PP/thermal	43.84
HDPE/HZSM-5	43.17
LDPE/HZSM-5	44.92
PP/HZSM-5	44.73
HDPE/FCC catalyst	45.83
LDPE/FCC catalyst	45.47
PP/FCC catalyst	45.52

presence of the catalysts increased the rates of plastic decomposition and vapor formation. As the vapors exited the reactor rapidly, there was insufficient time for extensive cracking of hydrocarbon molecules into smaller hydrocarbon compounds.

3.3.3. Compositions of liquid products

The GC/MS chromatograms (Figs. S2-S7) reveal a significant number of hydrocarbons in the liquid products. A tall peak that corresponds to the C6 compound in all chromatograms could be attributed to the hexane used for cleaning of autosampler of the GC instrument. Therefore, the percentage of C6 compounds in the liquid products was not analysed to prevent data misinterpretations. The presence of doublets and triplet peaks in the chromatograms signifies the presence of alkadienes, alkenes, and alkanes with similar carbon numbers in the liquid samples, which is a typical characteristic of plastic pyrolysis products [18,51]. Detailed information on the liquid product compositions is provided in Table S2 (Supplementary materials). To simplify the data analysis, the abundance of alkanes, alkenes, and aromatic compounds in the liquid products is illustrated in Fig. 9, whereas the details of the compounds in the liquid products are provided in Table S1. A careful examination of the chromatograms shows that catalytic pyrolysis of HDPE and LDPE possessed similar product distributions, while the liquid products from PP pyrolysis showed different product characteristics. This is clear evidence of the influence of plastic structures on the product formation route during pyrolysis.

The type of catalyst used in plastic pyrolysis also has an apparent influence on the liquid product compositions. Liquid products from catalytic pyrolysis of HDPE and LDPE over HZSM-5 contained hydrocarbons with carbon numbers in C7-C15, represented by the tall peaks in the chromatograms (Figs. S3–4). HZSM-5 produced a high amount of aromatic compounds in the liquid products from the three plastics pyrolyzed. This observation is related to the high abundance of benzene, toluene, ethylbenzene, xylene and naphthalenes. HDPE pyrolysis produces an exceptionally high percentage of aromatic compounds (93.0 %) at the expense of alkenes (5.5 %) and alkanes (1.49 %). A similar trend is observed for LDPE pyrolysis, which produced 74.8 % aromatic compounds, 18.2 % alkenes, and 7.0 % alkanes. The considerably high proportion of naphthalene in the liquid products is related to the extensive cyclization of pyrolysis intermediates catalyzed by HZSM-5 [59]. A slightly different trend is observed for PP pyrolysis, which produced considerably more alkenes (38.3 %) and alkanes (16.9 %) and fewer aromatic compounds (44.9 %) (Fig. S5). Past investigations show that the highly acidic and microporous structure of HZSM-5 zeolite promotes β-scissions of C-C bonds along the polymer chain to produce carbonium ions and olefinic compounds. The carbonium ions can undergo further β-scissions to produce smaller oligomers, followed by isomerization, oligomerization, cyclization and aromatization of the oligomers, forming a wide range of hydrocarbon compounds [60]. The bulky structures of PP molecules hinder effective contact of the molecules with the catalyst particles, leading the decreased cyclization and aromatization. Due to the high contents of aromatics (mainly C7-C8 compounds), the plastic pyrolysis liquid products over HZSM-5 possess low average molecular weight (AMM) (9.73–11.14).

The chromatograms representing catalytic pyrolysis over FCC catalyst (Figs. S6-S8) show different trends to those over HZSM-5. All the liquid products contain C5-C35 hydrocarbons, represented by peaks with lower heights. Such observations indicate a wide product distribution. As FCC catalysts possess lower surface area and weaker acidity than those of HZSM-5, the catalyst was incapable of producing small hydrocarbons with narrow product distribution. Catalytic pyrolysis of plastics over FCC catalyst produced liquid products that contained more alkenes (38.3–67.6 %) and alkanes (16.9–25.1 %), with a small number of aromatic compounds (6.7–9.5 %). Catalytic pyrolysis of HDPE and LDPE produced a slightly higher amount of C19-C40 alkanes (13.4–15.6 % compared to PP, 7.9 %), while catalytic pyrolysis of PP produced a slightly higher amount of C9-C19 compounds (11.0 % compared to HDPE and LDPE, 8.5–9.7 %). Therefore, the AMM of the liquid products over the FCC catalyst are higher (21.74–22.49) than those over HZSM-5. No apparent difference was observed in terms of the abundance of aromatic compounds according to carbon number. These observations show that the strength and density of Brønsted acidic sites play a more

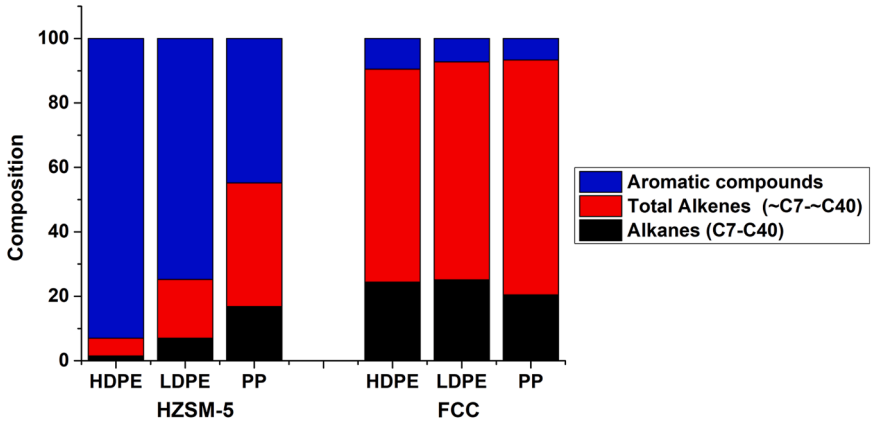

Fig. 9. Composition of liquid products from catalytic pyrolysis.

critical role than the BET surface area in the aromatization of plastic pyrolysis intermediates. The effects of plastic-type exerted minor influences on the liquid product distribution in this case.

3.4. Catalyst deactivation

The temperature-programmed oxidation of the catalysts used in plastic pyrolysis provides qualitative and quantitative information on the amount and types of cokes formed on the catalysts. Fig. 10 indicate different coking behaviors on the spent catalysts. For the HZSM-5 zeolite, 2–3 peaks were observed (in addition to the peak at ~100 °C which signifies moisture presence). This observation indicates the formation of different types of cokes that (i) can be decomposed at lower temperatures (150–330 °C), and (ii) can be decomposed at higher temperatures (330–760 °C). In general, cokes are formed via the aromatization of hydrocarbon oligomers on Brønsted acidic sites. Investigations on plastic pyrolysis [61] and alkene aromatization [62] demonstrated that cokes could exist in the spaces between the catalyst

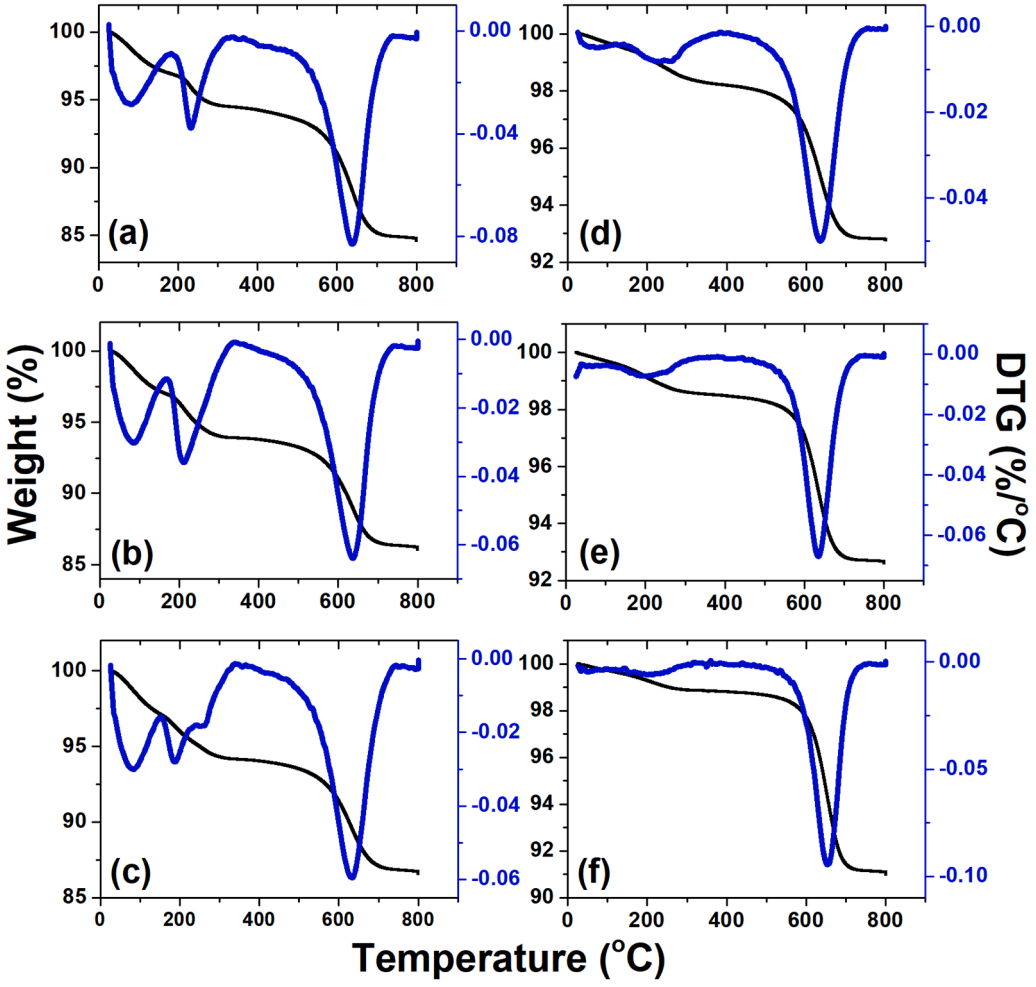

Fig. 10. TGA and DTG curves for regeneration of coked catalysts used in the catalytic pyrolysis of (a) HDPE over HZSM-5, (b) LDPE over HZSM-5, (c) PP over HZSM-5, (d) HDPE over FCC catalyst, (e) LDPE over FCC catalyst, and (f) PP over FCC catalyst.

particles or on the catalyst surface (termed soft coke), or inside the catalyst micropores, where the Brønsted acidic sites are located (termed hard coke). Soft coke consists mostly of oligomers and can be removed via heating in an inert environment. In contrast, hard coke is a poly-aromatic hydrocarbon formed via hydrogen transfer, isomerization, cyclization, and aromatization of plastic cracking products on the Brønsted acidic sites [63]. Due to the more complex structure of the hard coke, higher temperatures are required for its complete oxidation.

For the HZSM-5 zeolites, the coke yields are 2.36 %, 2.14 %, and 2.18 % for HDPE, LDPE, and PP, respectively, concerning the mass of plastic samples pyrolyzed. For the FCC catalyst, coke decomposition produced peaks at similar positions to those observed on ZSM zeolites. Strong peaks at ~640 °C were observed in all the FCC catalyst samples, irrespective of the plastic type. In contrast, small peaks were observed at 220–240 °C on the FCC catalyst used for HDPE and LDPE pyrolysis. The peak is almost non-existent for the FCC catalyst used for PP pyrolysis. The strong peak observed at ~640 °C is attributed to the coke formed on the weak acidic sites of the FCC catalyst. The coke yields are 1.32 %, 1.38 % and 1.70 % for HDPE, LDPE, and PP, respectively. The characterization results in Section 3.2 indicate the almost non-existence of the strong acidic sites in the regenerated FCC catalyst (Table 2). The formation of coke, despite in small amount, shows that the sites played a non-negligible role during plastic pyrolysis. The difference in the coke yields observed in HZSM-5 zeolite and FCC catalysts are attributed to the higher density and strengths of Brønsted acidic sites in the former catalyst. The high acidity of HZSM-5 is known to aromatize plastic volatiles, which leads to coke formation. The rapid deactivation of HZSM-5 in plastic pyrolysis remains an issue that requires innovative solutions [51]. A more detailed study is required to unravel the possible influence of plastic-type on the catalyst coking behavior.

3.5. Analysis of the electrical energy consumption

To illustrate the advantage of induction heating in plastic pyrolysis, the electrical energy consumed by the induction heater during plastic pyrolysis was measured using a C.A 8436 Qualistar+ Power Quality analyser (Chauvin Arnoux). Measurements under different conditions show that the electrical energy consumption was independent of the masses of plastics and catalysts during pyrolysis (as heat energy was supplied in excess to the reaction system) and was only related to the induction heater power and reactor dimensions. The electrical energy consumed during 10 min of plastic pyrolysis was 228 kJ (≈63.4 Wh) (Fig. S9a, Supplementary materials). This value is significantly lower than those recorded by Wu et al. [64] for biomass pyrolysis, namely 665.2 kJ at 550 °C (with the presence of metal hollow balls) and 819.9 kJ (without the presence of metal hollow balls) at 600 °C. The observed difference could be attributed to the smaller size of the reactor heated in this study (reactor diameter: 2.2 cm, length of the reactor to be inductively heated: 5.0 cm) when compared to the reactor used by Wu et al. [64] (reactor diameter: 5.6 cm, length of the reactor to be inductively heated: not specified).

As plastic/biomass pyrolysis using induction heating is rarely reported in scientific literature, data on the electrical energy consumption of the process is scarce. To provide a direct comparison, electrical energy consumption during plastic pyrolysis in a fixed bed reactor using an electric furnace (based on resistive heating) was also measured using the power quality analyser. In contrast to the reactor heating profile depicted in Fig. S1, a long heating time (25 min) is required to raise the reactor temperature to ~650 °C, followed by plastic pyrolysis for 10 min. These steps consumed 1225.8 kJ (340.5 Wh) and 270 kJ (75.1 Wh) respectively, resulting in total energy consumption of 1535 kJ (426.4 Wh) (Fig. S9b, Supplementary materials). The measurement values indicate an 85 % saving in electrical energy consumption when plastic pyrolysis is performed via induction heating over resistive heating. These values indicate the potential energy saving for plastic pyrolysis via induction heating. A similar observation was also made by Okan et al. [65], where sewage sludge pyrolysis driven by induction heating (4.62 MJ/kg) consumed less energy than resistive heating (6.65 MJ/kg) under similar reaction conditions. A more accurate comparison of energy consumption in plastic pyrolysis using induction heating and resistive heating will be necessary using the same reactor which can be inductively and resistively heated.

In this study, the reactor was heated to a high temperature at a reaction time sufficient to ensure complete plastic conversion. Therefore, the heat energy supplied to the system was in excess compared to the theoretical energy needed to depolymerize the plastic pellets. This statement implies that the electrical energy consumption per unit mass of reactant would decrease at a higher reactant loading, as suggested by Okan et al. [65]. The energy efficiency of the plastic pyrolysis via induction heating can be improved when the potential effects of reaction parameters (frequency of the alternating magnetic field generated by the induction heater, current used for induction heater, the magnetic permeability of the reactor material etc.) which affects reactor temperature during induction heating are fully understood. Statistical process optimization is another strategy to increase the energy efficiency of the plastic pyrolysis process.

3.6. Potentials and challenges of inductively heated plastic pyrolysis

In literature, different reactor designs have been proposed for plastic pyrolysis to maximize conversion and liquid/gas yields, while minimizing coke formation on catalysts [66,67]. Plastic pyrolysis in batch and semi-batch reactors exhibit satisfactory process performance at the laboratory scale and provide scientists with ample information on the process performance. Nevertheless, the development of reactor designs that allow continuous operation mode is essential to enable process scale-up. In addition, significant energy consumption and long heating time are recognized as a few of the technical challenges in plastic pyrolysis. Microwave-assisted pyrolysis is proven to be an excellent strategy to overcome the aforementioned challenges, as the heat energy can be rapidly produced from metallic susceptors inside the reactor vessel [68], which minimizes the heating/cooling time and energy losses to the surroundings. In addition, the heat transfer limitation can be minimized, as the susceptors are mixed with the plastic feed. Due to the incompatibility with the stainless-steel reactor, microwave-assisted pyrolysis is typically performed in a specialized reaction system, which contains a reactor vessel made of microwave-transparent materials (quartz/ceramic). The limited mechanical strengths of these materials restrain the prospects of microwave-assisted pyrolysis in the plastic recycling sector, especially when considering the possible pressure fluctuations due to the volatile gases released during the process. This study presents the possibility to conduct plastic pyrolysis in a stainless-steel fixed-bed reactor in an alternating magnetic field. The reactor was heated up to 650 °C within 10 min, which was sufficient for complete plastic conversion. Due to the short residence time of plastic pyrolysis intermediates in the reactor heating zone, thermal pyrolysis produced mainly wax products with a small amount of hydrocarbon gas. The addition of zeolitic catalysts significantly improved the yields of gas and liquid products at the expense of the wax product. The product yields and compositions, as well as the catalyst deactivation behaviors, can be explained with references to past investigations on plastic pyrolysis using resistive heating and microwave heating. This exploratory study demonstrates the feasibility of plastic pyrolysis via induction heating of a reaction vessel, which is comparable to microwave heating in terms of heating/cooling time. The use of a stainless-steel reactor allows possible pressure variation during the process, hence increasing the safety margin when considering the process upscaling potential. The avoidance of metallic susceptors in the plastic feed could lead to a more convenient treatment of solid residue in the reactor after plastic pyrolysis. These findings also demonstrate the high flexibility of the inductively heated plastic pyrolysis system in plastic waste valorization into various products, depending on the desired end-uses and market value

of these products. It is believed that the application of induction heating can be extended to various existing reactor designs (auger reactor [69], conical spouted bed reactor [70], vertical falling film reactor [71], among others) and process designs (pyrolysis, gasification [72], hydrothermal processing [73] among others), which is an interesting option to improve energy efficiency while retaining the unique advantages related to these reactor/process designs. Nevertheless, more fundamental studies are needed for a comprehensive understanding and control of inductively heated plastic pyrolysis. The lack of data on the yields of H_2, as well as C5 and C6 compounds in plastic pyrolysis products in this study, is a significant shortcoming that will be tackled in future studies.

4. Conclusions

The study examined the feasibility of induction heating in the thermal and catalytic pyrolysis of HDPE, LDPE, and PP plastics using two HZSM-5 (MFI topology) and FCC (FAU topology) catalysts, which has not been explored in the literature. In all the experimental runs, the plastic conversion started within 3–5 min of reaction time, and complete plastic conversion was observed within 10 min. This observation corresponded to the rapid reactor temperature increase upon induction heating. Thermal pyrolysis produced a significant amount of wax (72.4–73.9 wt%) and a small amount of non-condensable gas products (rich in C3 followed by C2 compounds). The presence of the catalysts significantly enhanced the gas (70.6–73.9 wt% for HZSM-5 and 62.4–75.2 wt% for FCC catalyst) and liquid yield (24.0–27.2 wt% for HZSM-5 and 0–35.9 wt% for FCC catalyst), at the expense of wax yield (0 wt% for HZSM-5 and 0 −25.4 wt% for FCC catalyst). The gas products for the catalytic pyrolysis were rich in C3 followed by C4 compounds, regardless of the plastic and catalyst properties. On the other hand, a significant variation in terms of liquid product distribution is observed for catalytic pyrolysis. HZSM-5 zeolite produced liquid products with high aromatics content, especially C7-C10 aromatics (representing toluene, ethylbenzene, xylene, naphthalene and several alkylbenzene isomers). The FCC catalyst produced a high number of liquid products, which were richer in alkenes and alkanes in the C9-C40 range. The outlined differences are attributed to the different textural properties and acidity profiles of the catalysts, which led to different reaction pathways during plastic pyrolysis. These observations validate the ability of the catalysts in product distribution modification despite the short residence time. Polymer types also influenced product yields and distribution, in agreement with past investigations in plastic pyrolysis. Coke analysis revealed the formation of cokes (2.14–2.38 wt% for HZSM-5 and 1.32 – 1.70 wt% for FCC catalyst) of different strengths, corresponding to the different acidic sites on the catalysts. Based on the similar decomposition peaks of these cokes in HZSM-5 and FCC catalysts, it is hypothesized that the cokes were formed on the strong and weak acidic sites of these zeolitic catalysts.

To conclude, this exploratory study demonstrates the feasibility of new pyrolysis powered by induction heating in the production of different value-added products from plastics. The adoption of induction heating could be an interesting strategy that reduces the time needed for plastic waste pyrolysis, especially at a larger scale. In addition, the prospects of applying induction heating on stainless-steel reactors also provide an interesting scaling-up strategy that allows possible pressure variation. As induction heating is also known to have higher energy conversion efficiency than resistive heating, future studies will be dedicated to the quantification of energy consumption in plastic pyrolysis assisted with induction heating.

CRediT authorship contribution statement

Syie Luing Wong: Investigation, Methodology, Writing – original draft. **Sabino Armenise:** Conceptualization, Validation. **Bemgba Bevan Nyakuma:** Writing – reviewing and editing. **Anna Bogush:** Formal analysis, Data curation. **Sam Towers:** Formal analysis, Data curation. **Chia Hau Lee:** Software, Resources. **Keng Yinn Wong:** Software, Resources. **Ting Hun Lee:** Software. **Evgeny Rebrov:** methodology, Supervision. **Marta Muñoz:** Supervision, Project administration, Funding acquisition.

Declaration of Competing Interest

The authors declare that they have no known competing financial interests or personal relationships that could have appeared to influence the work reported in this paper.

Data availability

Data will be made available on request.

Acknowledgment

Syie Luing Wong and Sabino Armenise have received support from the European Union's Horizon 2020 research and innovation program under the Marie Skłodowska-Curie grant Agreement No. 754382, GOT ENERGY TALENT. The content of this publication does not reflect the official opinion of the European Union. Responsibility for the information and views expressed in this paper lies entirely with the authors. Marta Muñoz also gratefully acknowledges the financial support from the Comunidad de Madrid (S2018/NMT-4411) for a project titled "Additive Manufacturing: from Material to Application." Syie Luing Wong wishes to thank John Pillier, Li SiRui, Joe Gregory, and Deema Kunda for all the guidance and assistance provided during his research associated with the School of Engineering, University of Warwick, UK. Syie Luing Wong and Sabino Armenise also acknowledge the contributions of Carlos Prieto and the FCC team from CEPSA to this study in terms of materials, technical analysis, and intellectual discussions.

Appendix A. Supporting information

Supplementary data associated with this article can be found in the online version at doi:10.1016/j.jaap.2022.105793.

References

[1] W.W.Y. Lau, Y. Shiran, R.M. Bailey, E. Cook, M.R. Stuchtey, J. Koskella, C.A. Velis, L. Godfrey, J. Boucher, M.B. Murphy, R.C. Thompson, E. Jankowska, A. Castillo Castillo, T.D. Pilditch, B. Dixon, L. Koerselman, E. Kosior, E. Favoino, J. Gutberlet, S. Baulch, M.E. Atreya, D. Fischer, K.K. He, M.M. Petit, U.R. Sumaila, E. Neil, M. V. Bernhofen, K. Lawrence, J.E. Palardy, Evaluating scenarios toward zero plastic pollution, Science 369 (2020) 1455, https://doi.org/10.1126/science.aba9475.

[2] S.L. Wong, B.B. Nyakuma, K.Y. Wong, C.T. Lee, T.H. Lee, C.H. Lee, Microplastics and nanoplastics in global food webs: a bibliometric analysis (2009-2019), Mar. Pollut. Bull. 158 (2020), 111432, https://doi.org/10.1016/j.marpolbul.2020.111432.

[3] L.A. Hamilton, S. Feit, C. Muffett, M. Kelso, S.M. Rubright, C. Bernhardt, E. Schaeffer, D. Moon, J. Morris and R. Labbé-Bellas2019. Plastic & climate: the hidden costs of a plastic planet. ⟨https://www.ciel.org/wp-content/uploads/2019/05/Plastic-and-Climate-FINAL-2019.pdf⟩, 2019 (accessed 05/04/2022).

[4] M. De Smet, M. Linder, R. Koopmans, Kv Doorsselaer, C. Velis, B. De Wilde, A.-C. Ritschkoff, M. Crippa, J. Leyssens and M.M. Wagner, Jane2019. A circular economy for plastics – insights from research and innovation to inform policy and funding decisions. ⟨https://op.europa.eu/en/publication-detail/-/publication/33251cf9–3b0b-11e9–8d04–01aa75ed71a1/language-en/format-PDF⟩, 2019 (accessed 15/11/2020).

[5] S. Armenise, S. Wong, J.M. Ramírez-Velásquez, F. Launay, D. Wuebben, B. B. Nyakuma, J. Rams, M. Muñoz, Application of computational approach in plastic pyrolysis kinetic modelling: a review, React. Kinet. Mech. Catal. 134 (2021) 591, https://doi.org/10.1007/s11144-021-02093-7.

[6] Closed Loop Partners2021. Accelerating circular supply chains for plastics: a landscape of transformational technologies that stop plastic waste, keep materials in play and grow markets. ⟨https://www.closedlooppartners.com/wp-content/uploads/2021/01/CLP_Circular_Supply_Chains_for_Plastics_Updated.pdf⟩, 2021 (accessed 23/03/2022).

[7] S.L. Wong, G.R. Mong, B.B. Nyakuma, N. Ngadi, K.Y. Wong, M.M. Hernández, S. Armenise, C.T. Chong, Upcycling of plastic waste to carbon nanomaterials: a

bibliometric analysis (2000–2019), Clean. Technol. Environ. Policy 24 (2022) 739, https://doi.org/10.1007/s10098-021-02267-w.
[8] S. Armenise, W. SyieLuing, J.M. Ramírez-Velásquez, F. Launay, D. Wuebben, N. Ngadi, J. Rams, M. Muñoz, Plastic waste recycling via pyrolysis: a bibliometric survey and literature review, J. Anal. Appl. Pyrolysis 158 (2021), 105265, https://doi.org/10.1016/j.jaap.2021.105265.
[9] SusChem 2020. Strategic innovation and research agenda (SIRA). ⟨https://suschem.org/files/library/SIRA-2020/SusChem_SIRA_07_02_V02_interactif.pdf⟩, 2020 (accessed 15 November 2020).
[10] SusChem2020. Sustainable plastics strategy. ⟨http://suschem.org/files/library/Publications/Suschem_Sustainable_Plastics_Brochure-FINAL_2101.pdf⟩, 2020 (accessed 23/03/2022).
[11] W.T. Tsai, J.H. Chang, K.J. Hsien, Y.M. Chang, Production of pyrolytic liquids from industrial sewage sludges in an induction-heating reactor, Bioresour. Technol. 100 (2009) 406, https://doi.org/10.1016/j.biortech.2008.06.013.
[12] P.D. Muley, C. Henkel, K.K. Abdollahi, D. Boldor, Pyrolysis and catalytic upgrading of pinewood sawdust using an induction heating reactor, Energy Fuels 29 (2015) 7375, https://doi.org/10.1021/acs.energyfuels.5b01878.
[13] H. Mishra, B. Patidar, A.S. Pante, A. Sharma, Mathematical modelling, simulation and experimental validation of resistance heating and induction heating techniques for E-waste treatment, IET Electr. Power Appl. 13 (2019) 487, https://doi.org/10.1049/iet-epa.2018.5535.
[14] K. Nakanoh, S. Hayashi, K. Kida, Waste treatment using induction heated pyrolysis, Fuji Electr. Rev. 47 (2001) 69.
[15] J. Zeaiter, A process study on the pyrolysis of waste polyethylene, Fuel 133 (2014) 276, https://doi.org/10.1016/j.fuel.2014.05.028.
[16] Y. Qiu, X. Hou, G. Liu, L. Wang, X. Zhang, Fast recovery of Brønsted acid sites lost during high-temperature calcination in HZSM-5, Microporous Mesoporous Mater. 243 (2017) 176, https://doi.org/10.1016/j.micromeso.2017.02.030.
[17] O. Mazaheri, R.J. Kalbasi, Preparation and characterization of Ni/mZSM-5 zeolite with a hierarchical pore structure by using KIT-6 as silica template: an efficient bi-functional catalyst for the reduction of nitro aromatic compounds, RSC Adv. 5 (2015), 34398, https://doi.org/10.1039/c5ra02349a.
[18] I. Dubdub, M. Al-Yaari, Pyrolysis of low density polyethylene: kinetic study using TGA data and ANN prediction, Polymers 12 (2020) 891, https://doi.org/10.3390/polym12040891.
[19] J. Baena-Gonzalez, A. Santamaria-Echart, J.L. Aguirre, S. Gonzalez, Chemical recycling of plastic waste: bitumen, solvents, and polystyrene from pyrolysis oil, Waste Manag. 118 (2020) 139, https://doi.org/10.1016/j.wasman.2020.08.035.
[20] B.R.G. Leliveld, M.J.H.V. Kerkhoffs, F.A. Broersma, J.A.J. van Dillen, J.W. Geus, D. C. Koningsberger, Acidic properties of synthetic saponites studied by pyridine IR and TPD-TG of n-propylamine, J. Chem. Soc., Faraday Trans. 94 (1998) 315, https://doi.org/10.1039/a705357f.
[21] S. Wong, N. Ngadi, T.A. Tuan Abdullah, I.M. Inuwa, Catalytic cracking of LDPE dissolved in benzene using nickel-impregnated zeolites, Ind. Eng. Chem. Res. 55 (2016) 2543, https://doi.org/10.1021/acs.iecr.5b04518.
[22] D. Barik (Ed.), Energy From Toxic Organic Waste for Heat and Power Generation, Woodhead Publishing, 2019, p. 17. ⟨https://www.sciencedirect.com/science/article/pii/B9780081025284000031⟩.
[23] D. Xu, Y. Xiong, J. Ye, Y. Su, Q. Dong, S. Zhang, Performances of syngas production and deposited coke regulation during co-gasification of biomass and plastic wastes over Ni/γ-Al2O3 catalyst: Role of biomass to plastic ratio in feedstock, Chem. Eng. J. 392 (2020), 123728, https://doi.org/10.1016/j.cej.2019.123728.
[24] B. Fekhar, V. Zsinka, N. Miskolczi, Value added hydrocarbons obtained by pyrolysis of contaminated waste plastics in horizontal tubular reactor: In situ upgrading of the products by chlorine capture, J. Clean. Prod. 241 (2019), 118166, https://doi.org/10.1016/j.jclepro.2019.118166.
[25] B. Fekhar, L. Gombor, N. Miskolczi, Pyrolysis of chlorine contaminated municipal plastic waste: In-situ upgrading of pyrolysis oils by Ni/ZSM-5, Ni/SAPO-11, red mud and Ca(OH)2 containing catalysts, J. Energy Inst. 92 (2019) 1270, https://doi.org/10.1016/j.joei.2018.10.007.
[26] K. Ding, S. Liu, Y. Huang, S. Liu, N. Zhou, P. Peng, Y. Wang, P. Chen, R. Ruan, Catalytic microwave-assisted pyrolysis of plastic waste over NiO and HY for gasoline-range hydrocarbons production, Energy Convers. Manag. 196 (2019) 1316, https://doi.org/10.1016/j.enconman.2019.07.001.
[27] S. Klaimy, J.F. Lamonier, M. Casetta, S. Heymans, S. Duquesne, Recycling of plastic waste using flash pyrolysis – effect of mixture composition, Polym. Degrad. Stab. 187 (2021), 109540, https://doi.org/10.1016/j.polymdegradstab.2021.109540.
[28] L. Shafigullin, N. Romanova, I. Gumerov, A. Gabrakhmanov and D. Sarimov,2018. Thermal properties of polypropylene and polyethylene blends (PP/LDPE), at: IOP Conference Series: Materials Science and Engineering, 012070.
[29] I. Dubdub, M. Al-Yaari, Pyrolysis of mixed plastic waste: I. Kinetic study, Materials 13 (2020) 4912, https://doi.org/10.3390/ma13214912.
[30] C.A. Cáceres, L. Zborowski, S.V. Canevarolo, Thermo-mechanical degradation and VOC emission of unstabilized and stabilized polypropylene copolymer during multiple extrusions, Mater. Res. 14 (2011) 569, https://doi.org/10.1590/s1516-14392011005000081.
[31] H.-X. Zhang, Y.-J. Lee, J.-R. Park, D.-H. Lee, K.-B. Yoon, Control of molecular weight distribution for polypropylene obtained by commercial ziegler-natta catalyst: effect of electron donor, Macromol. Res. 19 (2011) 622, https://doi.org/10.1007/s13233-011-0614-5.
[32] J.S. Fabiyi, A.G. McDonald, Degradation of polypropylene in naturally and artificially weathered plastic matrix composites, Maderas, Cienc. Y. Tecnol. 16 (2014) 0, https://doi.org/10.4067/s0718-221×2014005000021.
[33] M. Arabiourrutia, G. Elordi, G. Lopez, E. Borsella, J. Bilbao, M. Olazar, Characterization of the waxes obtained by the pyrolysis of polyolefin plastics in a conical spouted bed reactor, J. Anal. Appl. Pyrolysis 94 (2012) 230, https://doi.org/10.1016/j.jaap.2011.12.012.
[34] X. Xian, J. Chen, Y. Chu, M. He, S. Zhao, L. Dong, J. Ren, Unraveling the spatial distribution of the acidity of HZSM-5 zeolite on the level of crystal grains, AlChE J. 67 (2021), e17134, https://doi.org/10.1002/aic.17134.
[35] D.K. Ojha, R. Vinu, Resource recovery via catalytic fast pyrolysis of polystyrene using zeolites, J. Anal. Appl. Pyrolysis 113 (2015) 349, https://doi.org/10.1016/j.jaap.2015.02.024.
[36] X. Xian, M. He, Y. Gao, Y. Bi, Y. Chu, J. Chen, L. Dong, J. Wang, S. Zhao, Acidity tuning of HZSM-5 zeolite by neutralization titration for coke inhibition in supercritical catalytic cracking of n-dodecane, Appl. Catal. A: Gen. 623 (2021), 118278, https://doi.org/10.1016/j.apcata.2021.118278.
[37] G. Caeiro, P. Magnoux, J.M. Lopes, F.R. Ribeiro, S.M.C. Menezes, A.F. Costa, H. S. Cerqueira, Stabilization effect of phosphorus on steamed H-MFI zeolites, Appl. Catal., A: Gen. 314 (2006) 160, https://doi.org/10.1016/j.apcata.2006.08.016.
[38] M. Milina, S. Mitchell, N.-L. Michels, J. Kenvin, J. Pérez-Ramírez, Interdependence between porosity, acidity, and catalytic performance in hierarchical ZSM-5 zeolites prepared by post-synthetic modification, J. Catal. 308 (2013) 398, https://doi.org/10.1016/j.jcat.2013.08.020.
[39] P. Losch, G. Laugel, J.S. Martinez-Espin, S. Chavan, U. Olsbye, B. Louis, Phosphorous modified ZSM-5 zeolites: impact on methanol conversion into olefins, Top. Catal. 58 (2015) 826, https://doi.org/10.1007/s11244-015-0449-y.
[40] N.L.A. Souza, I. Tkach, E. Morgado, K. Krambrock, Vanadium poisoning of FCC catalysts: a quantitative analysis of impregnated and real equilibrium catalysts, Appl. Catal. A: Gen. 560 (2018) 206, https://doi.org/10.1016/j.apcata.2018.05.003.
[41] U.J. Etim, P. Bai, X. Liu, F. Subhan, R. Ullah, Z. Yan, Vanadium and nickel deposition on FCC catalyst: influence of residual catalyst acidity on catalytic products, Microporous Mesoporous Mater. 273 (2019) 276, https://doi.org/10.1016/j.micromeso.2018.07.011.
[42] M. Thommes, K. Kaneko, A.V. Neimark, J.P. Olivier, F. Rodriguez-Reinoso, J. Rouquerol, K.S.W. Sing, Physisorption of gases, with special reference to the evaluation of surface area and pore size distribution (IUPAC technical report), Pure Appl. Chem. 87 (2015) 1051, https://doi.org/10.1515/pac-2014-1117.
[43] T.C. Hoff, D.W. Gardner, R. Thilakaratne, K. Wang, T.W. Hansen, R.C. Brown, J. P. Tessonnier, Tailoring ZSM-5 zeolites for the fast pyrolysis of biomass to aromatic hydrocarbons, ChemSusChem 9 (2016) 1473, https://doi.org/10.1002/cssc.201600186.
[44] S. Fu, Q. Fang, A. Li, Z. Li, J. Han, X. Dang, W. Han, Accurate characterization of full pore size distribution of tight sandstones by low-temperature nitrogen gas adsorption and high-pressure mercury intrusion combination method, Energy Sci. Eng. 9 (2020) 80, https://doi.org/10.1002/ese3.817.
[45] L. Wu, X. Li, Z. Yuan, Y. Chen, Fabrication and characterization of titanate nanotube supported ZSM-5 zeolite composite catalyst for ethanol dehydration to ethylene, Bull. Korean Chem. Soc. 35 (2014) 525, https://doi.org/10.5012/bkcs.2014.35.2.525.
[46] A.S. Barbosa, L.A. Siqueira, R.L. Medeiros, D.M. Melo, M.A. Melo, J.C. Freitas, R. M. Braga, Renewable aromatics through catalytic flash pyrolysis of pineapple crown leaves using HZSM-5 synthesized with RHA and diatomite, Waste Manag. 88 (2019) 347.
[47] S.K. Jesudoss, J.J. Vijaya, K. Kaviyarasu, L.J. Kennedy, R. Jothi Ramalingam, H. A. Al-Lohedan, Anti-cancer activity of hierarchical ZSM-5 zeolites synthesized from rice-based waste materials, RSC Adv. 8 (2018) 481, https://doi.org/10.1039/c7ra11763a.
[48] L. Wei, H. Chen, Y. Wei, J. Jia, R. Zhang, Ce-promoted Mn/ZSM-5 catalysts for highly efficient decomposition of ozone, J. Environ. Sci. 103 (2021) 219, https://doi.org/10.1016/j.jes.2020.10.008.
[49] C. Chen, J. Yu, B.A. Yoza, Q.X. Li, G. Wang, A novel "wastes-treat-wastes" technology: role and potential of spent fluid catalytic cracking catalyst assisted ozonation of petrochemical wastewater, J. Environ. Manag. 152 (2015) 58, https://doi.org/10.1016/j.jenvman.2015.01.022.
[50] S.A. Salaudeen, S.M. Al-Salem, S. Sharma, A. Dutta, Pyrolysis of high-density polyethylene in a fluidized bed reactor: pyro-wax and gas analysis, Ind. Eng. Chem. Res. 60 (2021) 18283, https://doi.org/10.1021/acs.iecr.1c03373.
[51] N. Zhou, L. Dai, Y. Lv, H. Li, W. Deng, F. Guo, P. Chen, H. Lei, R. Ruan, Catalytic pyrolysis of plastic wastes in a continuous microwave assisted pyrolysis system for fuel production, Chem. Eng. J. 418 (2021), 129412, https://doi.org/10.1016/j.cej.2021.129412.
[52] B. Whajah, N. da Silva Moura, J. Blanchard, S. Wicker, K. Gandar, J.A. Dorman, K. M. Dooley, Catalytic depolymerization of waste polyolefins by induction heating: selective alkane/alkene production, Ind. Eng. Chem. Res. 60 (2021) 15141, https://doi.org/10.1021/acs.iecr.1c02674.
[53] A. Hassani, Pyrolysis of plastic waste into green fuels–experimental study, Universitetet i Sørøst-Norge, Faculty of Technology, Nat. Sci. Marit. Sci. (2018) 86.
[54] M.S. Cahyono, U.Ika Fenti, Influence of heating rate and temperature on the yield and properties of pyrolysis oil obtained from waste plastic bag, Conserve.: J. Energy Environ. Stud. 1 (2017) 1, https://doi.org/10.30588/cjees.v1i1.248.
[55] S. Erdogan, in: B. Llamas, M.F.O. Romero, E. Sillero (Eds.), Sustainable Mobility, IntechOpen, London, 2020. ⟨https://www.intechopen.com/chapters/70583⟩.
[56] I. Ahmad, M.I. Khan, H. Khan, M. Ishaq, R. Tariq, K. Gul, W. Ahmad, Pyrolysis study of polypropylene and polyethylene into premium oil products, Int. J. Green. Energy 12 (2014) 663, https://doi.org/10.1080/15435075.2014.880146.
[57] X. Li, Y. Pang, Z. Ding, J. Li, X. Jiang, Y. Luo, H. Zhang, F. Zhu, Y. Wang, Enhancing the synergistic effect of cellulose and polypropylene for petrochemical production during catalytic fast pyrolysis by mesoporous gallium-MFI zeolites, Energy Fuels 35 (2021) 19525, https://doi.org/10.1021/acs.energyfuels.1c02627.

[58] H. Palza, C. Aravena, M. Colet, Role of the catalyst in the pyrolysis of polyolefin mixtures and used tires, Energy Fuels 31 (2017) 3111, https://doi.org/10.1021/acs.energyfuels.6b02660.
[59] Z. Sebestyén, M. Blazsó, E. Jakab, N. Miskolczi, J. Bozi, Z. Czégény, Thermo-catalytic studies on a mixture of plastic waste and biomass, J. Therm. Anal. Calorim. 147 (2021) 6259, https://doi.org/10.1007/s10973-021-10962-5.
[60] U. Khalil, Z. Liu, C. Peng, N. Hikichi, T. Wakihara, J. García-Martínez, T. Okubo, S. Bhattacharya, Ultrafast surfactant-templating of *BEA zeolite: an efficient catalyst for the cracking of polyethylene pyrolysis vapours, Chem. Eng. J. 412 (2021), 128566, https://doi.org/10.1016/j.cej.2021.128566.
[61] M.M. Hasan, N. Batalha, G. Fraga, M.H.M. Ahmed, L. Pinard, M. Konarova, S. Pratt, B. Laycock, Zeolite shape selectivity impact on LDPE and PP catalytic pyrolysis products and coke nature, Sustain. Energy Fuels 6 (2022) 1587, https://doi.org/10.1039/d2se00146b.
[62] M. Díaz, E. Epelde, J. Valecillos, S. Izaddoust, A.T. Aguayo, J. Bilbao, Coke deactivation and regeneration of HZSM-5 zeolite catalysts in the oligomerization of 1-butene, Appl. Catal., B: Environ. 291 (2021), 120076, https://doi.org/10.1016/j.apcatb.2021.120076.
[63] S. Tamiyakul, S. Anutamjarikun, S. Jongpatiwut, The effect of Ga and Zn over HZSM-5 on the transformation of palm fatty acid distillate (PFAD) to aromatics, Catal. Commun. 74 (2016) 49, https://doi.org/10.1016/j.catcom.2015.11.002.
[64] L. Wu, H. Ma, J. Mei, Y. Li, Q. Xu, Z. Li, Low energy consumption and high quality bio-fuels production via in-situ fast pyrolysis of reed straw by adding metallic particles in an induction heating reactor, Int. J. Hydrog. Energy 47 (2022) 5828, https://doi.org/10.1016/j.ijhydene.2021.11.229.
[65] M. Okan, H.M. Aydin, M. Barsbay, Current approaches to waste polymer utilization and minimization: a review, J. Chem. Technol. Biotechnol. 94 (2019) 8, https://doi.org/10.1002/jctb.5778.
[66] S.L. Wong, N. Ngadi, T.A.T. Abdullah, I.M. Inuwa, Current state and future prospects of plastic waste as source of fuel: a review, Renew. Sust. Energy Rev. 50 (2015) 1167, https://doi.org/10.1016/j.rser.2015.04.063.
[67] D.G. Kulas, A. Zolghadr, D.R. Shonnard, Liquid-fed waste plastic pyrolysis pilot plant: effect of reactor volume on product yields, J. Anal. Appl. Pyrolysis 166 (2022), 105601, https://doi.org/10.1016/j.jaap.2022.105601.
[68] Y. Liu, W. Fu, T. Liu, Y. Zhang, B. Li, Microwave pyrolysis of polyethylene terephthalate (PET) plastic bottle sheets for energy recovery, J. Anal. Appl. Pyrolysis 161 (2022), 105414, https://doi.org/10.1016/j.jaap.2021.105414.
[69] K.-B. Park, Y.-S. Jeong, J.-S. Kim, Activator-assisted pyrolysis of polypropylene, Appl. Energy 253 (2019), 113558, https://doi.org/10.1016/j.apenergy.2019.113558.
[70] S. Orozco, J. Alvarez, G. Lopez, M. Artetxe, J. Bilbao, M. Olazar, Pyrolysis of plastic wastes in a fountain confined conical spouted bed reactor: determination of stable operating conditions, Energy Convers. Manag. 229 (2021), 113768, https://doi.org/10.1016/j.enconman.2020.113768.
[71] Z. Jin, D. Chen, L. Yin, Y. Hu, H. Zhu, L. Hong, Molten waste plastic pyrolysis in a vertical falling film reactor and the influence of temperature on the pyrolysis products, Chin. J. Chem. Eng. 26 (2018) 400, https://doi.org/10.1016/j.cjche.2017.08.001.
[72] D. Saebea, P. Ruengrit, A. Arpornwichanop, Y. Patcharavorachot, Gasification of plastic waste for synthesis gas production, Energy Rep. 6 (2020) 202, https://doi.org/10.1016/j.egyr.2019.08.043.
[73] K. Jin, P. Vozka, G. Kilaz, W.-T. Chen, N.-H.L. Wang, Conversion of polyethylene waste into clean fuels and waxes via hydrothermal processing (HTP), Fuel 273 (2020), 117726, https://doi.org/10.1016/j.fuel.2020.117726.